Monodisperse monocomponent fuel droplet heating and evaporation

T Kristyadi, Valérie Deprédurand, Guillaume Castanet, Fabrice Lemoine, Sergei S. Sazhin, A Elwardany, Elena M. Sazhina, Morgan R. Heikal

Monodisperse monocomponent fuel droplet heating and evaporation

T. Kristyadi [a], V. Deprédurand [b], G. Castanet [b], F. Lemoine [b], S.S. Sazhin [c,*], A. Elwardany [c], E.M. Sazhina [c], M.R. Heikal [c]

[a] Mechanical Engineering Department, National Institute of Technology of Bandung, Jl PHH Mustofa No. 23, Bandung, Indonesia
[b] LEMTA, Nancy-Université, 2, Avenue de la Forêt de Haye, BP 160, 54504 Vandoeuvre-lès-Nancy, France
[c] Sir Harry Ricardo Laboratories, Centre for Automotive Engineering, School of Environment and Technology, Faculty of Science and Engineering, University of Brighton, Brighton BN2 4GJ, UK

Keywords:
Droplets
Heating
Evaporation
Fuels
Monodisperse spray

A B S T R A C T

The results of numerical and experimental studies of heating and evaporation of monodisperse acetone, ethanol, 3-pentanone, *n*-heptane, *n*-decane and *n*-dodecane droplets in an ambient air of fixed temperature and atmospheric pressure are reported. The numerical model took into account the finite thermal conductivity of droplets and recirculation inside them based on the effective thermal conductivity model and the analytical solution to the heat conduction equation inside droplets. The effects of interaction between droplets are taken into account based on the experimentally determined corrections to Nusselt and Sherwood numbers. It is pointed out that the interactions between droplets lead to noticeable reduction of their heating in the case of ethanol, 3-pentanone, *n*-heptane, *n*-decane and *n*-dodecane droplets, and reduction of their cooling in the case of acetone. Although the trends of experimentally observed droplet temperatures and radii are the same as predicted by the model taking into account the interaction between droplets, the actual values of the predicted droplet temperatures can differ from the observed ones by up to about 8 K, and the actual values of the predicted droplet radii can differ from the observed ones by up to about 2%. It is concluded that the effective thermal conductivity model, based on the analytical solution to the heat conduction equation inside droplets, can predict the observed average temperature of droplets with possible errors not exceeding several K, and observed droplet radii with possible errors not exceeding 2% in most cases. These results allow us to recommend the implementation of this model into CFD codes and to use it for multidimensional modelling of spray heating and evaporation based on these codes.

1. Introduction

The practical importance of accurate and computer efficient modelling of fuel droplet heating and evaporation in engineering applications is universally recognised (e.g. [1–3]). In most computational fluid dynamics (CFD) codes, this heating has been modelled assuming that there is no temperature gradient inside droplets (e.g. [4]). This assumption contradicts direct measurements of the temperature distribution inside droplets [5,6]. Bertoli and na Migliaccio [7] were perhaps the first to draw attention to the fact that taking into account the temperature gradient inside droplets can considerably increase the accuracy of the CFD modelling of combustion processes in Diesel engines. The analysis by these authors was based on the numerical solution of the heat conduction equation inside droplets. An alternative approach was suggested and developed in [8–13]. In these papers both finite liquid thermal conductivity and recirculation inside droplets (via the effective thermal conductivity (ETC) model [14]) were taken into account by incorporating the analytical solution to the heat conduction equation inside the droplet into the numerical scheme. This approach was shown to be considerably more efficient (from the points of view of both accuracy and computer efficiency) than the one used in [7].

The preliminary validation of the model developed in [8–12] against published experimental data was reported in [9]. This validation, however, was limited to the comparison of predicted and calculated droplet diameters or global characteristics such as the ignition delay. A more direct validation of the model, based on the comparison of the predictions of the model and the results of simultaneous measurement of average temperatures and diameters of monodisperse monocomponent droplets, was reported in [6]. The latter comparison, however, was limited to just two substances: ethanol and acetone in two different experimental conditions. The aim of this paper is to perform a comparison between the predictions of the model and experimental data, similar to the one reported in [6] but for a wider range of substances and different experimental conditions. The substances to be considered

* Corresponding author. Tel.: +44 1273 642677; fax: +44 1273 642301.
E-mail address: S.Sazhin@brighton.ac.uk (S.S. Sazhin).

are: acetone, ethanol, 3-pentanone, *n*-heptane, *n*-decane and *n*-dodecane. The experimental data used in our analysis are the same as earlier reported in [15]. These data were used in [15] for validation of the model different from the one developed in [8–12] (see [16,17]). Hence, this paper is complementary to both earlier published papers [6,15].

The model used in our analysis is briefly summarised in Section 2. The formulae derived earlier will be simplified, where possible, and presented in the format actually used in the numerical code. The experimental setup is briefly described in Section 3. In Section 4 the predictions of the model are compared with experimental data. The main results of the paper are summarised in Section 5.

2. Model

In the case when the convection heat transfer coefficient $h(t) = h = \text{const}$, the solution of the transient heat conduction equation with $R_d = \text{const}$ and the corresponding boundary and initial conditions, applied to a small time step $\Delta t = t_1 - t_0$ gives the following value of temperature at the end of the time step t_1 [8]:

$$T(R, t_1) = \frac{R_d}{R} \sum_{n=1}^{\infty} \Lambda_n \sin(\lambda_n R/R_d) + T_{\text{eff}}(t_1), \tag{1}$$

where:

$$\Lambda_n = \left[q_n - \frac{\mu_0(t_0) \sin \lambda_n}{\|\nu_n\|^2 \lambda_n^2} \right] \exp\left[-\kappa_0 \lambda_n^2 t_1\right] - \frac{\sin \lambda_n}{\kappa_0 \|\nu_n\|^2 \lambda_n^4} \left. \frac{\mathrm{d}\mu_0(t)}{\mathrm{d}t} \right|_{t=t_0} (1 - \exp\left[-\kappa_0 \lambda_n^2 (t_1 - t_0)\right]), \tag{2}$$

$$\mu_0(t) = \frac{h T_{\text{eff}}(t) R_d}{k_l}, \quad h_0 = (h R_d / k_l) - 1, \quad \|\nu_n\|^2 = \frac{1}{2}\left(1 + \frac{h_0}{h_0^2 + \lambda_n^2}\right),$$

$$\kappa_0 = \frac{k_l}{c_l \rho_l R_d^2}, \quad T_{\text{eff}} = T_g + \frac{\rho_l L \dot{R}_d}{h},$$

$$q_n = \frac{1}{\|\nu_n\|^2} \int_0^1 r T_0(r R_d) \sin(r \lambda_n) \mathrm{d}r,$$

a set of positive eigenvalues λ_n numbered in ascending order $(n = 1, 2, \ldots)$ is found from the solution of the following equation $\lambda \cos \lambda + h_0 \sin \lambda = 0$. If $T_0(R)$ is twice continuously differentiable, then the series in (1) converges absolutely and uniformly for all $t \geqslant 0$ and $R \in [0, R_d]$. When deriving (2) we assumed that the changes of $\frac{\mathrm{d}\mu_0(t)}{\mathrm{d}t}$ during the time step can be ignored. Ten terms in the series (1) were used in calculations. The effective thermal conductivity model was used in the case when the internal recirculation inside droplets is accounted [14]. The actual change of droplet radius is calculated as:

$$\dot{R}_d = \dot{R}_{dT} + \dot{R}_{dE}, \tag{3}$$

where $\dot{R}_{dT}$ is the change of droplet radius due to thermal expansion. The value of $\dot{R}_{dE}$ is controlled by fuel vapour diffusion from the droplet surface. It can be found from equation [11]:

$$\dot{m}_d = 4\pi R_d^2 \dot{R}_{dE} \rho_l = -2\pi \bar{\rho}_g D_{Fa} R_d \text{Sh}_0 \ln(1 + B_M), \tag{4}$$

where $\bar{\rho}_g$ is the average gas density (the contribution of fuel vapour to $\bar{\rho}_g$ has been ignored), D_{Fa} is the binary diffusion coefficient of fuel vapour in air (see [12]), $\text{Sh}_0 \equiv 2h_m R_d / D_{Fa}$ is the Sherwood number of non-evaporating droplets, h_m is the mass transfer coefficient. $B_M = (Y_{fs} - Y_\infty)/(1 - Y_{fs})$ is the Spalding mass transfer number, Y_{fs} and $Y_{f\infty}$ are the mass fractions of vapour near the droplet surface and at large distances from the droplet respectively. They are calculated from the Clausius–Clapeyron equation [19].

The Abramzon and Sirignano [14] model for the Sherwood and Nusselt numbers has been used. The values of the transport coefficients were taken for air at the temperature [11,18]: $T_{\text{ref}} = T_g + (T_g - T_s)/3$. The contribution of fuel vapour to the transport properties of air and the effects of droplets on air were ignored.

3. Experimental setup

Droplet diameters and average temperatures were measured using the experimental setup at the University of Nancy, which is described in a number of papers and theses, including [15–17]. This will be only briefly summarised below.

Linear monodisperse droplet streams are generated by Rayleigh disintegration of a liquid jet undergoing vibrations generated in a piezoelectric ceramic. The fuel is pre-heated in the injector by means of externally heated circulating water. The temperature of the fuel is measured exactly at the injection point with a K type thermocouple situated within the injector body. For specific frequencies of forced mechanical vibration, the liquid jet breaks up into equally spaced and monosized droplets. By adjusting the liquid flow rate and the piezoceramic frequency, it is possible to increase the droplet spacing up to about six times the droplet diameter. This, however, is accompanied by a modification of droplet sizes. The droplets are then injected into an enclosure fed with hot air coming from an electrical heater. In order to limit the thermal losses, a resistive electrical wire is inserted within the enclosure wall so that the wall temperature can be regulated to match that of the entering air. A temperature of up to 673 K could be reached. Destabilization of the droplet stream by the air motion can be a critical issue in this experiment. The air velocity is therefore maintained at between 0.1 and 0.3 m/s and the air flow is quietened by forcing it to go through a drilled wall and metallic foam. The problem of vapour saturation must be considered carefully due to the moderate movement of the air and the finite dimension of the chamber which has an inner diameter of 10 cm and a height of 14 cm. An estimate of the diffusion length L_d can be obtained considering diffusivity D_{Fa} is of the order of 10^{-5} m^2/s and maximal diffusion duration t is equal to 25 ms. The latter corresponds to the time required for a droplet to be transported through the enclosure. Based on these data we have $L_d = \sqrt{D_{Fa} t} \approx 0.5$ mm which is negligible compared to the inner radius of the enclosure. This ensures non-saturated conditions. Additionally, glass windows have been mounted in the wall to provide optical access. The two-colour laser-induced thermometry [20] is used to characterize the droplet temperature. The method involves the seeding of the liquid fuel with a small quantity of a fluorescent tracer, pyromethene 597-C8. The ratio of the fluorescence intensity detected on two spectral bands is a function of the temperature regardless of laser intensity, time-dependent tracer concentration, and measurement volume [21]. The velocity of the droplets is measured by Laser Doppler Velocimetry using the same laser light source as for the fluorescence excitation. The droplet size reduction is determined using the light scattering in the forward direction, where a stationary interference pattern is created. The measurement of the angular interfringe provides an accurate measurement of the droplet diameter.

Six liquid fuels were tested: acetone, ethanol, 3-pentanone, *n*-heptane, *n*-decane and *n*-dodecane. The approximations for the binary diffusion coefficients for each are given and discussed in Appendix A. Other physical properties of *n*-heptane and *n*-dodecane were assumed to be the same as in [12] (most of these properties were approximated using data from [22,23]). The physical properties of *n*-decane were taken to be the same as in [24], while the properties of acetone, ethanol and 3-pentanone were taken from [17,22,25].

An investigation of a number of droplet streams was performed. The temperature, velocity and diameter of the droplets were measured simultaneously at each measurement point. The periodicity of the droplets in the chain and the steady-state nature of their stream allowed us to convert the droplet distance from the injector into time. In our analysis, we focused on the evolution of droplets' temperatures and radii, starting from the moment when the first droplet was observed near the entrance to the enclosure. By placing a thermocouple at different locations it was established that air temperature T_a did not vary inside the chamber. Hence, it was considered to be constant during each experiment in our modelling. The droplet absolute velocities were approximated as linear functions of time (measured from the moment of injection):

$$v_d = v_1 - v_2 t, \tag{5}$$

where constants v_1 and v_2 were determined for each experiment, alongside the ratios $\mathrm{Nu}_n = \mathrm{Nu}/\mathrm{Nu}_{\mathrm{iso}}$ and $\mathrm{Sh}_n = \mathrm{Sh}/\mathrm{Sh}_{\mathrm{iso}}$, describing the effects of interaction between droplets in the stream, where the subscript $_{\mathrm{iso}}$ refers to isolated droplets. The error of determination of v_d is comparable with the ambient air velocities up to 0.3 m/s. This justifies our assumption that the absolute droplet velocities, estimated by Eq. (5), are equal to droplet velocities relative to ambient air. These velocities are used for the estimation of the Nusselt and Sherwood numbers for isolated droplets.

The values of the Nusselt and Sherwood numbers were estimated based on simultaneous measurements of droplet sizes and mean temperatures. These measurements allowed us to evaluate heat fluxes responsible for droplet heating and evaporation rates. These rates, alongside the measured time evolution of droplet mean temperatures, were used for the estimate of the convective heat flux, responsible for droplet heating, and mass flux of fuel vapour leaving the droplet. The main difficulty in converting these estimates into the estimates of the Nusselt and Sherwood numbers relates to the fact that the surface droplet temperatures T_s were not directly measured and had to be estimated. This issue is addressed in [15,17], where an iterative approach based on a simplified analysis of the energy balance of evaporation was used. After the droplet surface temperatures were estimated, the values of the Nusselt and Sherwood numbers were derived from the estimated heat and mass fluxes. Using the values of these numbers for isolated droplets, calculated from the Abramzon and Sirignano [14] model, the values of Nu_n and Sh_n, presented in Table 1, were calculated.

Three experiments were performed with each fuel, except 3-pentanone, for which only two experiments were performed. The values of T_a, distance parameter C (ratio of the distance between droplets and their diameters), initial droplet diameters D_{d0} (measured directly when the first droplets near the entrance to the enclosure were observed), Nu_n, Sh_n, v_1 and v_2 for each experiment are presented in Table 1, alongside boiling and critical temperatures (T_b and T_c) for each substance [22]. The values of C are shown to indicate the closeness of droplets in our experiments. In contrast to [6] they were not used to estimate Nusselt and Sherwood numbers.

The uncertainties in the measurement of the droplet diameters are expected to be about ±0.5 μm in most cases and the uncertainties in the temperature measurements are expected to be about ±1 K. Depending on the fuel and the experimental conditions, the uncertainties in the estimates of Sh_n and Nu_n are expected to be between 2% and 25% [15]. However, in the case of *n*-decane and *n*-dodecane, which have particularly low volatility, the mass loss due to evaporation was so low that it was not possible to determine accurately a value for Sh_n. Therefore, for these cases, the values of Sh_n were not estimated experimentally and we assumed them to be equal to Nu_n.

4. Results

The plots of temperature versus time for Case 1 for acetone and *n*-heptane, calculated using our model and obtained in the experiment are shown in Figs. 1 and 2. The values of parameters shown in Table 1 were used in calculations. The calculations were performed ignoring the interactions between droplets (indicated by subscript $_{\mathrm{iso}}$) and taking them into account, based on the values of Sh_n and Nu_n given in Table 1. Time in all figures is measured from the moment of injection.

Table 1
The values of T_a, C, D_{d0}, Nu_n, Sh_n, v_1 and v_2 for three experiments with acetone, ethanol, 3-pentanone, *n*-heptane, *n*-decane and *n*-dodecane droplets (abbreviated as acet, ethan, 3-pen, *n*-hep, *n*-dec and *n*-dod). The droplet velocities in m/s are approximated as $v_d = v_1 - v_2 t$, where t is in ms. In the case of *n*-decane and *n*-dodecane, the values of Sh_n were not estimated experimentally, but assumed to be equal to Nu_n.

Case	Parameter	Acet	Ethan	3-Pen	*n*-Hep	*n*-Dec	*n*-Dod
	T_b (K)	329.22	351.80	375.14	371.57	477.30	489.48
	T_c (K)	508.10	513.92	561.50	540.20	617.70	658.00
1	T_a (K)	640	643	634	644	643	643
1	C	4.5	4.3	4.9	4.4	3.7	4.6
1	D_{d0} (μm)	122.6	119.6	118.2	131.1	121.5	110.0
1	Nu_n	0.42	0.26	0.23	0.38	0.18	0.19
1	Sh_n	0.43	0.38	0.53	0.57	0.18	0.19
1	v_1 (m/s)	11.16	9.869	10.86	12.8	9.59	9.246
1	v_2 (m/(s · ms))	0.198	0.214	0.254	0.329	0.220	0.281
2	T_a (K)	645	643	645	645	645	644
2	C	5.5	6.1	4.0	5.3	4.4	6.9
2	D_{d0} (μm)	132.2	130.28	123.3	134.2	128.37	129.0
2	Nu_n	0.43	0.42	0.22	0.35	0.24	0.22
2	Sh_n	0.42	0.82	0.33	0.84	0.24	0.22
2	v_1 (m/s)	14.12	12.64	9.454	15.44	11.88	13.14
2	v_2 (m/(s · ms))	0.276	0.268	0.224	0.446	0.329	0.573
3	T_a (K)	647	644	n/a	647	647	643
3	C	3.3	3.1	n/a	3.8	5.4	3.0
3	D_{d0} (μm)	107.2	112.4	n/a	122.8	124.8	98.99
3	Nu_n	0.35	0.36	n/a	0.28	0.18	0.22
3	Sh_n	0.26	0.38	n/a	0.50	0.18	0.22
3	v_1 (m/s)	7.122	6.889	n/a	10.56	13.55	6.091
3	v_2 (m/(s · ms))	0.113	0.123	n/a	0.244	0.307	0.218

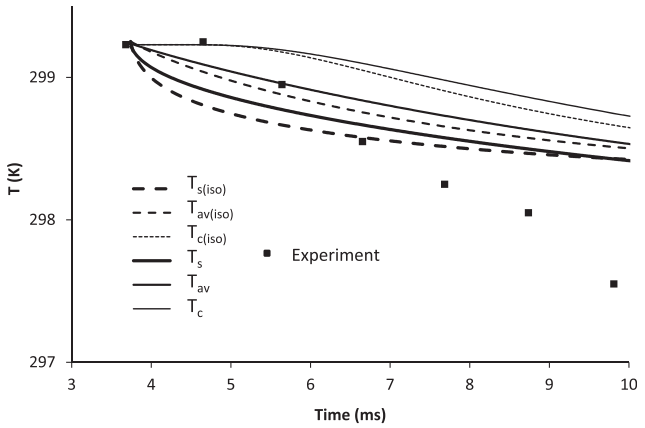

Fig. 1. Plots of the time evolution of the experimentally observed temperatures of acetone droplets for Case 1, and temperatures at the surface of these droplets (T_s), average temperatures in the droplets (T_{av}) and the temperatures at the centre of the droplets (T_c), predicted by the models ignoring the interactions between droplets (indicated by the subscript $_{iso}$), and taking into account these interactions. The input parameters of the models were taken from Table 1.

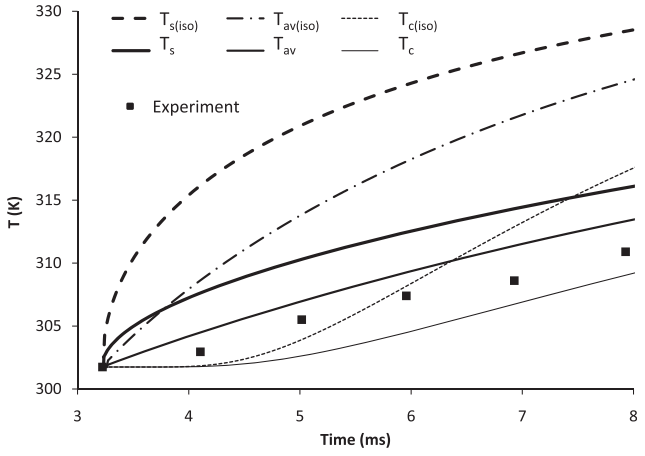

Fig. 2. The same as Fig. 1 but for *n*-heptane droplets.

The calculations started at the time when the droplets were first observed near the entrance to the chamber. The observed temperatures and radii of these droplets were used as the initial temperatures and radii in the model. It was assumed that initially there was no temperature gradient inside droplets.

As follows from Figs. 1 and 2, the plots referring to interacting and non-interacting (isolated) droplets are noticeably different for both substances. Similarly, the plots referring to the temperatures at the centres of the droplets, average temperatures, and the temperatures at the surfaces of the droplets are well separated. This result is similar to the one reported in [6], and it shows the limitation of the assumption, which is widely used in CFD codes, that the gradient of temperature inside droplets can be ignored.

The observed temperatures of acetone droplets, shown in Fig. 1, look rather different from the ones predicted by the model. Note, however, that the difference between the average temperature, predicted by the model, taking into account the interaction between droplets (T_{av}), and the experimentally observed temperatures is always less than 1 K, and can be naturally attributed to the uncertainty of the measurements, and uncertainties of the input parameters used in calculations.

In the case of *n*-heptane and *n*-dodecane droplets, the closeness between the experimentally observed temperatures and T_{av} was the most visible, compared with other droplets. The best matching between the experimentally observed temperatures and T_{av} can be seen for *n*-heptane, as shown in Fig. 2. However, even in this case, the actual deviation between these temperatures sometimes exceeds 1 K. This means that the model cannot predict the observed average droplet temperatures with errors less than about 1 K. For both these substances, the experimentally observed temperatures always lie between the temperatures T_s and T_c, predicted by the model, taking into account the interaction between droplets.

In the case of ethanol droplets the experimentally observed temperatures were closer to the ones predicted by the model, taking into account the interaction between droplets, than the one ignoring this interaction. However, the deviation between the experimental points and T_{av} for these droplets (up to about 3 K) was larger than in the case of acetone, *n*-heptane and *n*-dodecane droplets. The temperatures for 3-pentanone and *n*-decane were generally similar to those for ethanol, with the maximal deviation between the experimental points and T_{av} about 3 K for 3-pentanone and about 6 K for *n*-decane.

The plots of normalised droplet radii R_d/R_{d0} versus time for Case 1 for all six substances, calculated using our model and obtained in the experiment, are shown in Figs. 3 and 4. The initial values of droplet radii were taken to be equal to those for the droplets for which the first measurements of droplet temperature were taken.

When calculating the time evolution of R_d, both droplet evaporation and thermal expansion were taken into account based on Eq.

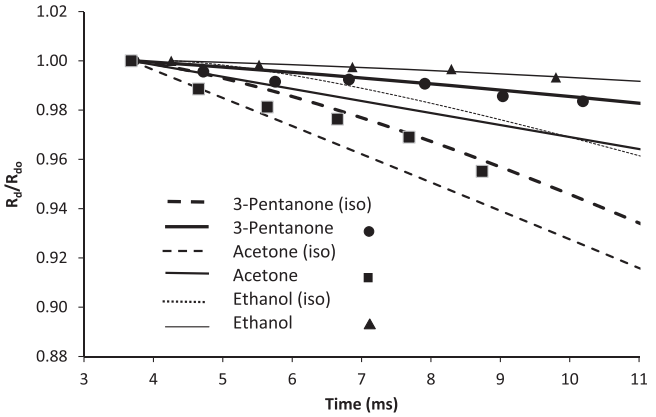

Fig. 3. Plots of the time evolution of the experimentally observed and modelled normalised droplet radii R_d/R_{d0} for acetone, ethanol and 3-pentanone droplets for Case 1. Models ignoring the interactions between droplets (indicated by the subscript $_{iso}$), and taking into account these interactions, were used. The input parameters of the models were taken from Table 1.

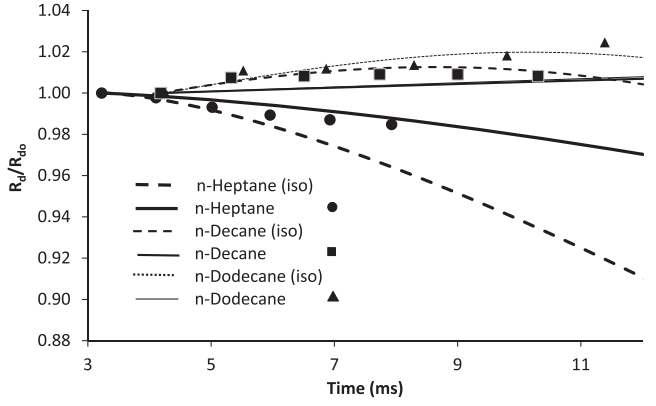

Fig. 4. The same as Fig. 3 but for *n*-heptane, *n*-decane and *n*-dodecane droplets.

(3). The values of parameters used for these calculations are given in Table 1. As follows from these figures, the plots referring to interacting and non-interacting droplets are noticeably different for all substances, as for the temperature plots shown in Figs. 1 and 2. Note that in contrast to [15] we presented the plots of the ratios of radii rather than the ratios of radii squared. The latter would have been justified if the analysis had been focused on droplet evaporation beyond the heat-up period, when the d^2-law is valid. In our case, however, the focus is on the heat-up period itself (cf. [26]).

As follows from Figs. 3 and 4, the effects of interaction between droplets lead to a decrease in the rate of reduction of their radii in the case of acetone, ethanol, 3-pentanone and *n*-heptane, but to a slowing down of the increase of these radii in the case of *n*-decane and *n*-dodecane. In the latter case, the effect of the thermal expansion of droplets dominates over the effects of evaporation. In the case of ethanol, 3-pentanone, *n*-heptane and *n*-decane the agreement between experimental plots and predictions of the model, taking into account the interaction between droplets, looks almost ideal. However, for acetone and *n*-dodecane the experimental data lie between the predictions of the models ignoring the interaction between droplets and taking them into account. Even in the case of these two substances, the deviation between the experimental results and the predictions of the model, taking into account the interaction between droplets, does not exceed about 2%.

For the results referring to Cases 2 and 3 we restricted our analysis to comparison of the experimental data with the average temperatures and R_d/R_{d0} predicted by the model taking into account the interaction between droplets, as was done in [15]. Instead of the actual droplet average temperatures T, studied for Case 1, the analysis for Cases 2 and 3 is focused on the difference between these temperatures and the initial droplet temperatures T_0. The corresponding plots for $T - T_0$ versus time for Case 2 for all six substances are shown in Fig. 5. As follows from this figure, although the trends predicted by the model are similar to the ones observed experimentally, there are noticeable deviations between the actual values of predicted and observed average droplet temperatures. The maximal deviation between them is seen for *n*-decane and *n*-dodecane droplets. The minimal deviation between them is seen for 3-pentanone droplets.

The plots of R_d/R_{d0} versus time for Case 2 for the same substances as in Fig. 5, are shown in Fig. 6. As one can see from this figure, the trends predicted by the model are similar to the ones

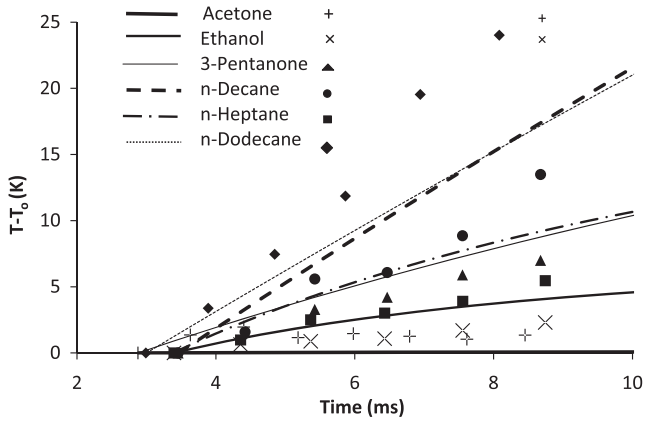

Fig. 5. Plots of the time evolution of the experimentally observed droplet temperatures $T - T_0$, where T_0 are the initial droplet temperatures, and the average temperatures of droplets, predicted by the model taking into account the interaction between droplets. The results for acetone, ethanol, 3-pentanone, *n*-heptane, *n*-decane and *n*-dodecane droplets for Case 2 are shown. The input parameters of the models were taken from Table 1.

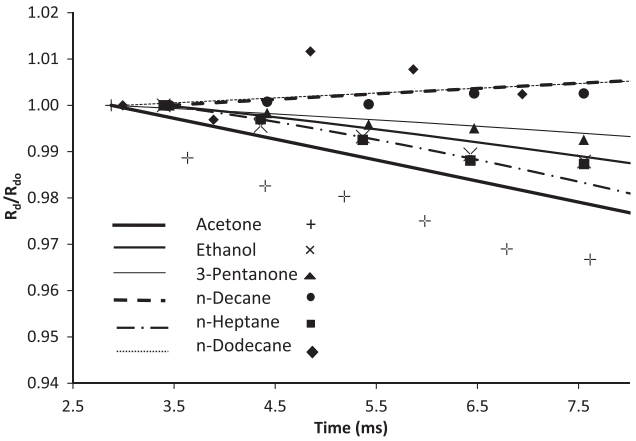

Fig. 6. The same as Fig. 5 but for R_d/R_{d0}.

observed experimentally, but there are noticeable deviations between the observed and predicted values of this ratio, as in the case of Fig. 5. The maximal deviation between these ratios (up to almost 2%) is seen for acetone droplets. The minimal deviation between these ratios is seen for 3-pentanone droplets. Hence, for Case 2 the best agreement between experimental and modelled results for both temperatures and radii is observed for 3-pentanone droplets.

The plots for $T - T_0$ versus time for Case 3 for acetone, ethanol, *n*-heptane, *n*-decane and *n*-dodecane (there is no data for 3-pentanone for Case 3) are shown in Fig. 7. As one can see from this figure, the agreement between experimental and modelled results is very good for acetone, while the deviation between the experimentally observed temperatures and those predicted by the model could reach more than about 5 K for ethanol and *n*-dodecane (although the observed and predicted trends for both substances are the same). The plots of R_d/R_{d0} versus time for Case 3 for the same substances as in Fig. 7, are shown in Fig. 8. As can be seen from this figure, the best agreement between experimental and modelled results can be seen for *n*-decane and *n*-heptane, and the worst for acetone and *n*-dodecane. However, even in the case of acetone and *n*-dodecane, both experimental and modelled results show the same trends and the deviation between them does not exceed 2%.

Several factors are expected to contribute to the difference between the modelled results presented in this paper and ones reported in [15,17]. Some approximations for transport coefficients used in this paper are different from those used in [15,17]. We used the time-averaged values of Nu_n and Sh_n, while both these parameters varied with time.

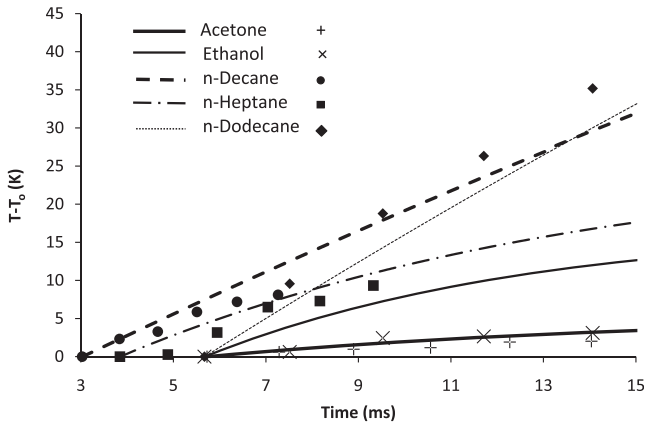

Fig. 7. The same as Fig. 5 but for Case 3, except without the results for *n*-pentanone.

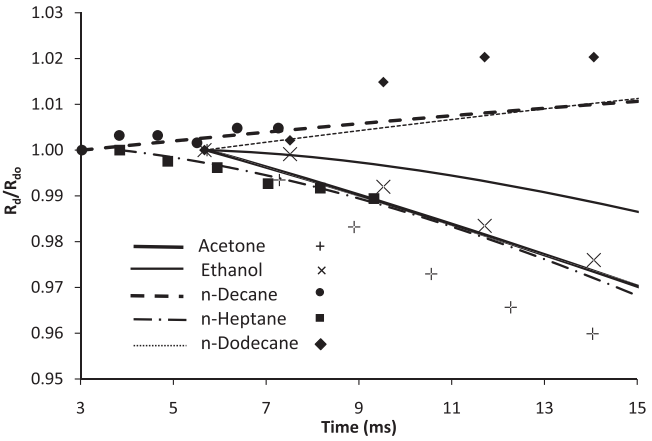

Fig. 8. The same as Fig. 7 but for R_d/R_{d0}.

5. Conclusions

Heating and evaporation of monodisperse acetone, ethanol, 3-pentanone, *n*-heptane, *n*-decane and *n*-dodecane droplets in ambient air at fixed temperature and atmospheric pressure have been studied numerically and experimentally. Droplet initial diameters varied from 99 to 135 μm, while ambient air temperatures varied from 634 to 647 K. The numerical model took into account the finite thermal conductivity of droplets and recirculation inside them based on the effective thermal conductivity model and the analytical solution to the heat conduction equation inside droplets. The initial values of droplet temperatures and radii were assumed to be equal to those observed experimentally for the first recorded droplet. It was assumed that initially there was no temperature gradient inside droplets.

It is pointed out that the interactions between droplets lead to noticeable reduction of their heating in the case of ethanol, 3-pentanone, *n*-heptane, *n*-decane and *n*-dodecane droplets, and enhancement of their cooling in the case of acetone. The interaction between droplets leads to a decrease in the rate of reduction of their radii in the case of acetone, ethanol, 3-pentanone and *n*-heptane, but to a slowing down of the increase of these radii in the case of *n*-decane and *n*-dodecane. In the latter case, the effect of the thermal expansion of droplets dominates over the effects of evaporation.

Although the trends of experimentally observed droplet temperatures and radii are the same as predicted by the model taking into account the interaction between droplets, the values of the predicted droplet temperatures can differ from the observed ones by up to about 8 K, and the actual values of the predicted droplet radii can differ from the observed ones by up to about 2%.

Combining the above results and those reported previously in [6] we can conclude that the effective thermal conductivity model, based on the analytical solution to the heat conduction equation inside droplets, can predict the observed average temperature of droplets with possible errors not exceeding several K, and observed droplet radii with possible errors not exceeding 2% in most cases. These results confirm our previous conclusion (see [9,10,12]) that this model can be recommended for implementation in CFD codes and used for multidimensional modelling of spray heating and evaporation based on these codes.

Acknowledgements

The authors are grateful to the Indonesian government (Academic Recharging Program) and the European Regional Development Fund Franco-British INTERREG IVA (Project C5, Reference 4005) for financial support of the work on this project.

Appendix A. Binary diffusion coefficient for fuel vapour

The binary diffusion coefficient for all fuels was estimated using the following equation [27]:

$$D_{Fa} = 1.8583 \times 10^{-7} \sqrt{T^3 \left(\frac{1}{M_F} + \frac{1}{M_a}\right)} \frac{1}{p\sigma_{Fa}^2 \Omega_{Fa}(T^*)}, \quad \text{(A1)}$$

where D_{Fa} is in m^2/s, p is in atm (1 atm = 0.101 MPa), T is in K, $\sigma_{Fa} = 0.5(\sigma_F + \sigma_a)$ is the minimal distance between molecules in Angström, Ω_{Fa} is the collision integral, the value of which depends on the normalised temperature $T^* = Tk_B/\epsilon$, k_B is the Boltzmann constant, $\epsilon = \sqrt{\epsilon_F \epsilon_a}$; the subscript $_a$ indicates air. Note that the formula for the binary diffusion coefficient used in [22] differs from the one presented above in terms of the value of the coefficient (they used 1.8623 instead of 1.8583). The difference between the values of this coefficient predicted by two formulae (0.2%) can be safely ignored in most practical applications. Note that there is a typo in Eq. (B5) of [12]. $\sigma_a = 3.617$ Angström, $\epsilon_a/k_B = 97.0$ K (Table E.1 in [27]). The values of these parameters and molar masses for acetone, ethanol, *n*-heptane, 3-pentanone and *n*-dodecane are given in Table A1.

There is some controversy regarding the values of σ_F and ϵ_F/k_B for *n*-heptane and *n*-dodecane. We used the data leading to the best fit with experimental data. These are indicated by * in the ϵ_F/k_B column.

Once the value of T^* had been found, the collision integral Ω_{Fa} could be obtained from Table E.2 [27]. However, we found it more convenient to use the analytical approximation of Ω_{Fa} given by Eq. (E.2-2) of [27]).

For the binary diffusion coefficient of *n*-decane ($C_{10}H_{22}$) we used the following approximation [24]:

$$D_{Fa} = 5.46 \times 10^{-6} \frac{1}{1.01\,p} \left(\frac{T}{300}\right), \quad \text{(A2)}$$

where p is in atm, as in Eq. (A1).

Table A1
The values of σ_F, ϵ_F/k_B and molar masses for acetone, ethanol, *n*-heptane, 3-pentanone and *n*-dodecane, as inferred from various sources.

Fuel	Reference	Formula	σ_F in Angström	ϵ_F/k_B in K	Molar mass in kg/kmole
Acetone	[22]	C_3H_6O	4.600	560.2	58.080
Ethanol	[22]	C_2H_6O	4.530	362.6	46.069
n-Heptane	[28,22]	C_7H_{16}	5.949	399.3*	100.204
n-Heptane	[27]	C_7H_{16}	6.663	352	100.20
n-Heptane	[29,22]	C_7H_{16}	6.498	455.04	46.069
3-Pentanone	[28,22]	$C_5H_{10}O$	4.22	351.562	86.134
n-Dodecane	[28,22]	$C_{12}H_{26}$	9.37	245.0	170.338
n-Dodecane	[29,22]	$C_{12}H_{26}$	6.5972	454.6768*	170.338

Data indicated by * in the ϵ_F/k_B column were used in our analysis.

References

[1] Polyanin AD, Kutepov AM, Vyazmin AV, Kazenin DA. Hydrodynamics mass and heat transfer in chemical engineering. London and New York: Taylor and Francis; 2002.

[2] Michaelides EE. Particles, bubbles and drops. Singapore: World Scientific; 2006.

[3] Faghri A, Zhang Y. Transport phenomena in multiphase systems. Burlington: Elsevier; 2006.

[4] Sazhina EM, Sazhin SS, Heikal MR, Babushok VI, Johns R. A detailed modelling of the spray ignition process in diesel engines. Combust Sci Technol 2000;160:317–44.

[5] Castanet G, Lebouché M, Lemoine F. Heat and mass transfer of combusting monodisperse droplets in a linear stream. Int J Heat Mass Trans 2005;48:3261–75.

[6] Maqua C, Castanet G, Grisch F, Lemoine F, Kristyadi T, Sazhin SS. Monodisperse droplet heating and evaporation: experimental study and modelling. Int J Heat Mass Trans 2008;51:3932–45.

[7] Bertoli C, na Migliaccio M. A finite conductivity model for diesel spray evaporation computations. Int J Heat Fluid Flow 1999;20:552–61.

[8] Sazhin SS, Krutitskii PA, Abdelghaffar WA, Sazhina EM, Mikhalovsky SV, Meikle ST, et al. Transient heating of diesel fuel droplets. Int J Heat Mass Trans 2004;47:3327–40.

[9] Sazhin SS, Abdelghaffar WA, Sazhina EM, Heikal MR. Models for droplet transient heating: effects on droplet evaporation, ignition, and break-up. Int J Therm Sci 2005;44:610–22.

[10] Sazhin SS, Abdelghaffar WA, Krutitskii PA, Sazhina EM, Heikal MR. New approaches to numerical modelling of droplet transient heating and evaporation. Int J Heat Mass Trans 2005;48:4215–28.

[11] Sazhin SS. Advanced models of fuel droplet heating and evaporation. Prog Energy Combust Sci 2006;32:162–214.

[12] Sazhin SS, Kristyadi T, Abdelghaffar WA, Heikal MR. Models for fuel droplet heating and evaporation: comparative analysis. Fuel 2006;85: 1613–30.

[13] Sazhin SS, Krutitskii PA, Martynov SB, Mason D, Heikal MR, Sazhina EM. Transient heating of a semitransparent spherical body. Int J Therm Sci 2007;46:444–57.

[14] Abramzon B, Sirignano WA. Droplet vaporization model for spray combustion calculations. Int J Heat Mass Trans 1989;32:1605–18.

[15] Deprédurand V, Castanet G, Lemoine F. Heat and mass transfer in evaporating droplets in interaction: influence of the fuel. Int J Heat Mass Trans 2010;53:3495–502.

[16] Castanet G. Etude aérothermique d'un jet de gouttes monodispersé en évaporation et en combustion à l'aide de méthodes optiques. Thèse présentée pour l'obtention du grade de Docteur de l'Université Henri Poincaré, Vandoeuvre-Les-Nancy; 2004.

[17] Deprédurand V. Approche experimentale de l' évaporation de sprays de combustibles multicomposants. Thèse présentée pour l'obtention du grade de Docteur de l'Institut National Polytechnique de Lorraine, Vandoeuvre-Les-Nancy; 2009.

[18] Incropera FP, DeWitt DP. Fundamentals of heat and mass transfer. 5th ed. John Wiley and Sons; 2002.

[19] Kuo KK. Principles of combustion. John Wiley and Sons; 1986.

[20] Lavieille P, Lemoine F, Lavergne G, Lebouché M. Evaporating and combusting droplet temperature measurements using two color laser induced fluorescence. Exp Fluids 2001;31:45–55.

[21] Deprédurand V, Miron P, Labergue A, Wolff M, Castanet G, Lemoine F. A temperature sensitive tracer suitable for two-colour laser-induced fluorescence thermometry applied to evaporating droplets. Measur Sci Technol 2008;19(10):1–12.

[22] Poling BE, Prausnitz JM, O'Connell J. The properties of gases and liquids. New York: McGraw-Hill; 2000.

[23] Maxwell JB. Data book on hydrocarbons: application to process engineering. New York: Van Nostrand Company, Inc.; 1950.

[24] Abramzon B, Sazhin S. Convective vaporization of fuel droplets with thermal radiation absorption. Fuel 2006;85:32–46.

[25] National Institute of Standards and Technology (NIST). Chemistry WebBook, 2010. <http://webbook.nist.gov/chemistry/>.

[26] Sazhin SS, Krutitskii PA, Gusev IG, Heikal M. Transient heating of an evaporating droplet. Int J Heat Mass Trans 2010;53:2826–36.

[27] Bird RB, Stewart EW, Lightfoot EN. Transport phenomena. 2nd ed. New York, Chichester: Wiley and Sons; 2002.

[28] Hirschfelder JO, Curtiss CF, Bird RB. Molecular theory of gases and liquids. 4th ed. New York, Chichester: John Wiley and Sons; 1967.

[29] Paredes MLL, Nobrega R, Tavares FW. A completely analytical equation of state for mixture of square-well chain fluid of variable well width. In: XIX Inter American Congress of Chemical Engineering, Agios de Sao Pedro, Brazil; 24–27 September 2000 [paper no. 396].